applied sciences

MDPI

Article

A Short-Circuit Current Calculation Model for Renewable Power Plants Considering Internal Topology

Po Li [1], Ying Huang [1,*], Guoteng Wang [1], Jianhua Li [2] and Jianyu Lu [2]

[1] College of Electrical Engineering, Zhejiang University, Hangzhou 310027, China; 12410072@zju.edu.cn (P.L.); wgt339@zju.edu.cn (G.W.)
[2] China East Branch of State Grid Corporation of China, Shanghai 200120, China; li_jianhua@ec.sgcc.com.cn (J.L.); lu_jy@ec.sgcc.com.cn (J.L.)
* Correspondence: huangyingzju@zju.edu.cn

Abstract: With the large-scale integration of renewable energy into the grid, traditional short-circuit current (SCC) calculation methods for synchronous generators are no longer applicable to inverter-based non-synchronous machine sources (N-SMSs). Current SCC calculation methods for N-SMSs often use a single-machine multiplication method, which tends to overlook the internal variability of N-SMSs within power plants, leading to low calculation accuracy. To address this issue, this paper first derives an analytical expression for SCC in grid-connected inverters under low voltage ride through (LVRT) control strategies. Then, a single-machine steady-state SCC calculation model is proposed. Based on the classification of N-SMSs, a practical SCC calculation model for renewable power plants is introduced, balancing accuracy and computational speed. The feasibility of the model is validated through simulations. The proposed method enables simple calculations to obtain the steady-state voltage and SCC at the machine terminal, offering strong engineering practicality.

Keywords: low voltage ride through; short-circuit current; inverter; renewable power plants; non-synchronous machine sources

Citation: Li, P.; Huang, Y.; Wang, G.; Li, J.; Lu, J. A Short-Circuit Current Calculation Model for Renewable Power Plants Considering Internal Topology. *Appl. Sci.* **2024**, *14*, 10745. https://doi.org/10.3390/app142210745

Received: 18 October 2024
Revised: 18 November 2024
Accepted: 18 November 2024
Published: 20 November 2024

1. Introduction

In recent years, with the large-scale integration of renewable energy into the power grid and the widespread application of high-voltage direct current (HVDC), the power system has been evolving toward a high proportion of power electronics [1], significantly altering the fault characteristics of traditional synchronous machine-dominated grids. When a short-circuit fault occurs in the power system, it is necessary to calculate the SCC for relay protection [2]. Unlike traditional synchronous generators, the SCC of renewable energy, which is integrated via converters, is influenced by control strategies [3,4].

Research on the SCC of N-SMSs, based on the fault progression, can be divided into transient and steady-state SCC studies. These studies mainly focus on constructing mathematical models of converters, deriving analytical expressions for SCC under different fault conditions, and examining the effects of pre-fault states, low-voltage ride through (LVRT) control strategies, and current-limiting parameters on steady-state SCC. For transient SCC, the control loops of converters are analyzed, and analytical expressions for SCC are derived through system transfer functions or differential equations [5–8]. Regarding steady-state SCC, control strategies for voltage source converters (VSCs) are introduced, and the impact of current-limiting values on SCC is analyzed [9]. A steady-state SCC calculation model for doubly fed and permanent magnet wind turbines is also developed, considering the effects of LVRT control strategies [10]. Typically, when calculating steady-state SCC, N-SMSs are modeled as voltage-controlled current sources based on LVRT control strategies. At present, research on single-machine SCC for N-SMSs is relatively comprehensive.

However, renewable power plants often comprise dozens or even hundreds of N-SMSs, making it impractical to construct detailed models and perform analytical SCC

calculations for each unit during faults. The main method currently used for calculating SCC in renewable power plants is the equivalent method. This study proposes a practical method called the single-machine multiplication method, combined with the traditional SCC calculation approach for synchronous generators, to introduce a local iterative method for the fault region [11]. Although the single-machine multiplication method simplifies the entire renewable power plant into an equivalent non-synchronous machine source, its simplicity comes at the cost of precision, as it neglects the internal variability of the wind turbines in the plant. Hence, accurate equivalent modeling of renewable power plants remains a key challenge. Existing equivalent modeling approaches typically reduce the complexity of renewable power plants based on specific parameters. Wind speed, rotor speed, stator voltage, and real-time active power are selected as clustering indicators, and the doubly fed induction generator is grouped using fuzzy C-means clustering [12]. The fault and fault transition process is discussed, and through the grouping of the active power ramp recovery control module, the photovoltaic power station is subjected to equivalent clustering [13]. One method classifies hybrid wind farms based on turbine types and control strategies [10]. Another method categorizes wind farms according to initial wind speed and steady-state terminal voltage during faults, achieving high accuracy but increasing computational complexity due to iterative calculations of terminal voltage [14]. A further approach analyzes the impact of fault severity and current limiters on active power output, grouping generation units based on the degree of voltage drop, which significantly improves accuracy compared to the single-machine multiplication method [15]. An iterative short-circuit current-voltage algorithm that considers the internal structural parameters of wind farms has been proposed, achieving substantial improvements in convergence, though it increases the number of iterations [16]. A quasi-Newton iterative algorithm is used to calculate the short-circuit current under high proportions of distributed power sources. While the power grid model with voltage and current mutual iteration has good overall calculation accuracy, it includes a large number of variables, making it time-consuming for large-scale wind farm integration [17]. However, due to the nonlinearity of voltage and current, the above calculation methods often rely on iterative processes, raising concerns about convergence and computational resource demands.

To address the aforementioned issues, this paper first introduces the control strategies of N-SMSs, and then, based on typical control strategies, derives analytical expressions for SCC. Subsequently, it analyzes the response characteristics and underlying mechanisms influencing SCC, establishing a single-machine SCC calculation model for N-SMSs. Furthermore, the paper proposes a method for calculating steady-state fault voltage at the grid connection point and, considering the internal structure of renewable power plants, develops an SCC calculation model for renewable power plants. Finally, the feasibility of the proposed SCC calculation method is verified through simulations in PSCAD/EMTDC.

2. Classification and Control Strategies of N-SMSs

2.1. Control Strategies of N-SMSs

The SCC calculation method proposed in this paper is closely related to the classification and control strategies of N-SMSs. Therefore, the control strategies for N-SMSs are introduced first.

The typical structure of a non-synchronous power source is shown in Figure 1 [18]. In Figure 1, U_{dc} represents the DC-side voltage of the voltage source converter (VSC), and u_v represents the AC bus voltage on the grid side of the VSC. At a macro level, N-SMSs can be categorized into two grid-connection modes: grid-following and grid-forming.

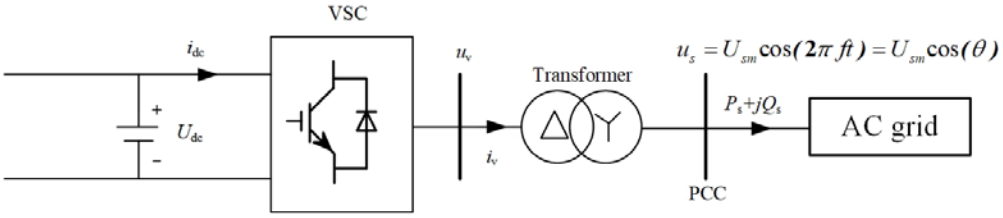

Figure 1. Typical structure of N-SMSs.

The primary distinction between grid-following and grid-forming N-SMSs lies in how they maintain synchronization with the grid. Grid-following sources use a phase-locked loop (PLL) to synchronize with the grid, which requires the grid-following N-SMSs to be connected to an active grid for operation. Grid-following N-SMSs can be further classified into two types based on their ability to support AC bus voltage: PV grid-following and PQ grid-following sources. Both types aim to maintain the DC-side voltage U_{dc} at a setpoint U_{dc}^* or the active power P_s at a setpoint P_s^*. The key difference between them is that the PV grid-following source aims to maintain the VSC grid-side bus voltage amplitude U_{sm} at a setpoint, U_{sm}^*, analogous to a PV node in power flow analysis. In contrast, the PQ grid-following source aims to maintain the reactive power output Q_s of the VSC at a setpoint, Q_s^*, which corresponds to a PQ node in power flow analysis.

On the other hand, grid-forming sources maintain synchronization with the grid via a power synchronization loop (PSL). Based on the adjustable range of active power, grid-forming N-SMSs can be further divided into two types: Vθ grid-forming and PV grid-forming sources. The difference between the two is that the PV grid-forming source can only operate when connected to an active grid.

The four types of N-SMSs mentioned above all utilize a three-loop controller structure, with the outermost loop tailored to their respective control objectives. The inner dual-loop controllers, however, are conventional inner-outer loop controllers, a control strategy that is well-established and widely adopted. These controllers typically adopt proportional-integral (PI) control. Taking the PQ grid-following non-synchronous power sources as an example, their control principle is illustrated in Figure 2, where the control equations for the dual-loop system are presented.

$$\begin{cases} u_d = (k_P + \frac{k_I}{s})(i_d^* - i_d) + Ri_{gd} - \omega Li_q + u_{gd} \\ u_q = (k_P + \frac{k_I}{s})(i_q^* - i_q) + Ri_{gq} + \omega Li_d + u_{gq} \\ i_{d0}^* = (k_{vP} + \frac{k_{vI}}{s})(u_{dc}^* - u_{dc}) \\ i_{q0}^* = 0 \end{cases} \quad (1)$$

where

- the superscript "*" denotes the reference values for the controller;
- u_d and u_q represent the d-axis and q-axis components of the inverter bridge output voltage;
- i_d and i_q denote the d-axis and q-axis components of the inverter output current;
- L and R are the AC-side filter inductance and resistance;
- ω is the synchronous angular velocity;
- k_{vP} and k_{vI} are the proportional and integral parameters of the voltage outer-loop controller, respectively;
- k_P and k_I are the proportional and integral parameters of the current inner-loop controller;
- u_{gd} and u_{gq} represent the d-axis and q-axis voltage components at the power source port;
- u_{dc} is the DC bus voltage of the inverter;
- i_{d0}^* and i_{q0}^* are the d-axis and q-axis current reference values under steady-state operating conditions.

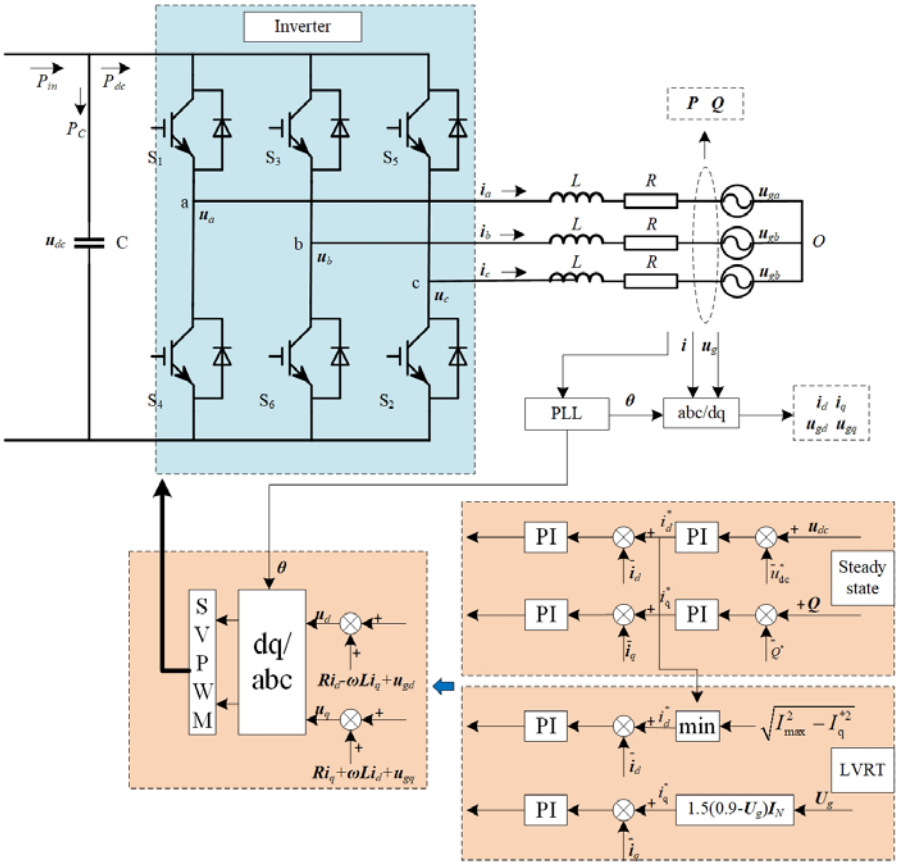

Figure 2. Diagram of grid connected inverter and its control system.

2.2. LVRT Control Strategy

During a short-circuit fault in the power grid, the terminal voltage of N-SMS drops, requiring these sources to supply reactive current to support the grid voltage. At this point, the voltage control outer loop is deactivated, and the reference values for the current inner loop are determined by the LVRT control strategy.

Taking wind farms as an example, according to the grid connection standards [19], during symmetrical faults, the LVRT requirements specify the provision of reactive current during the voltage dip period:

$$\Delta I_t = K_1 \times (0.9 - U_t) \times I_N, 0.2 \leq U_t \leq 0.9 \quad (2)$$

where

- ΔI_t represents the incremental dynamic reactive current injected by the wind farm;
- K_1 is the proportional coefficient of the dynamic reactive current for the wind farm, with a value range of no less than 1.5 and preferably no greater than 3;
- U_t is the per-unit value of the voltage at the point of grid connection for the wind farm;
- I_N is the rated current of the wind farm.

In this paper, K_1 is set to 1.5, and because the wind farm operates under a unit power factor condition, the reference value for the reactive current during the LVRT period can be derived as follows:

$$I_q{}^* = 1.5(0.9 - U_t)I_N, 0.2 \leq U_t \leq 0.9 \quad (3)$$

Due to the current limiting protection requirements of the inverter, the maximum value of the active current during the LVRT period is as follows:

$$I_{dmax}{}^* = \sqrt{I_{max}{}^2 - I_q{}^{*2}} \quad (4)$$

where

- $I_{\mathrm{dmax}}{}^{*}$ is the upper limit of the active current;
- I_{max} is the current limit of the inverter,
- $I_{\mathrm{q}}{}^{*}$ is the reference value of the reactive current.

At this point, the command value of the active current is the minimum between the pre-fault active current command value and $I_{\mathrm{dmax}}{}^{*}$. Therefore, the current inner loop command value during the LVRT period is as follows:

$$\begin{cases} i_{\mathrm{d}}{}^{*} = \min(i_{\mathrm{d0}}, I_{\mathrm{dmax}}{}^{*}) \\ i_{\mathrm{q}}{}^{*} = 1.5(0.9 - U_{\mathrm{t}})I_{\mathrm{N}} \end{cases} \tag{5}$$

The complete control block diagram is shown in Figure 2.

2.3. Response Characteristics of SCC in N-SMSs

During steady-state operation, the grid-connected converter of the N-SMSs adopts a steady-state grid connection control strategy, with a reactive power command of 0 to achieve unit power factor operation. When a short-circuit fault occurs externally to the N-SMSs, the voltage at the point of common coupling (PCC) drops. If the voltage falls to the threshold for LVRT, the converter control strategy switches to LVRT mode. At this point, the "power-voltage" outer loop of the dual-loop control structure is locked, and the command value for the current inner loop is directly given by (5). Consequently, the SCC response process during this period is determined by the parameters of the PI controller in the current inner loop, the transfer function of the converter, and the transfer function of the filtering circuit.

During the fault, only the command value of the current inner loop's PI controller changes. Therefore, investigating the time-domain response characteristics of the current inner loop is essential to consider its impact on the transient process of SCC.

Due to the control strategy employed to suppress negative-sequence currents, the reference value for negative-sequence current is set to zero during both normal operation and fault conditions. During faults, only the reference value for the positive-sequence current in the dual-PI current inner loop changes. Therefore, the impact of the positive-sequence current inner loop on the transient process of SCC is considered by studying its time-domain characteristics.

Figure 3 illustrates the structure of the q-axis current inner loop. The term $K_{\mathrm{ip}} + K_{\mathrm{ii}}/\mathrm{s}$ represents the transfer function of the PI controller in the current inner loop, where K_{ip} and K_{ii} are the proportional and integral coefficients, respectively. The term $K_{\mathrm{PWM}}/(T_{\mathrm{PWM}}/\mathrm{s}+1)$ represents the transfer function of the inverter, which is a first-order inertia element. Here, K_{PWM} is the inverter gain, and T_{PWM} is the inertia time constant. The term $1/(Ls + R)$ represents the transfer function of the terminal filtering circuit, where L, R are the inductance and resistance, respectively, of the connection between the terminal and the external grid.

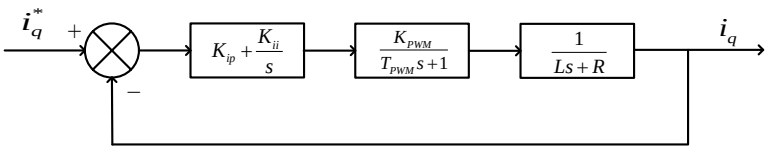

Figure 3. The positive-sequence q-axis current inner loop.

Based on this, the open-loop transfer function of the current inner loop can be written as follows:

$$\frac{i_{\mathrm{q}}}{i_{\mathrm{q}}{}^{*}} = G_{\mathrm{iq}}(s) = \frac{K_{\mathrm{PWM}}K_{\mathrm{ip}}(s + \frac{K_{\mathrm{ii}}}{K_{\mathrm{ip}}})}{sL(s + R/L)(sT_{\mathrm{PWM}} + \mathbf{1})} \tag{6}$$

After the fault, the reference current changes. Considering a typical unit step change, the output current is as follows:

$$i_{\mathrm{q}} = \frac{\mathbf{1}}{s}\frac{G_{\mathrm{iq}}(s)}{\mathbf{1} + G_{\mathrm{iq}}(s)} \tag{7}$$

A study [20] utilized fault recording data to verify the parameters of the current inner loop, resulting in a unit step response adjustment time of 8.5 ms for the current inner loop, as shown in Figure 4. This indicates that when the reference value experiences a step change after the fault, the current inner loop will control the output current to match the reference current value within several milliseconds, leading to a very short transient process. The SCC quickly transitions into a steady-state process after the fault. However, because the change in the reference value is not necessarily a step change, the actual response time of the current inner loop may be slightly longer. Simulations using a typical permanent magnet synchronous generator model show that the SCC enters a steady state in approximately 10 ms. The average response time of SF_6 circuit breakers is from 40 ms to 100 ms, providing a theoretical basis for determining the applicability of the proposed SCC calculation model.

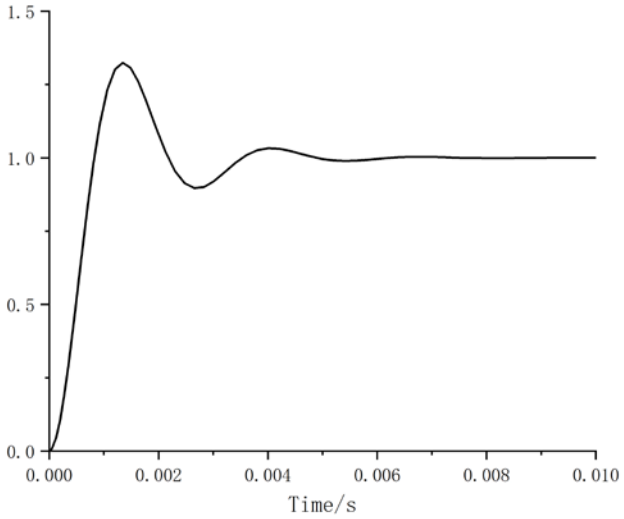

Figure 4. Current inner loop unit step response curve.

During the LVRT control period, as the voltage outer loop is deactivated, the current response is only influenced by the current loop. Neglecting the resistance, R, the analytical expression for the SCC during the fault period can be derived as follows [7]:

$$\begin{cases} i_{\mathrm{d}} = {i_{\mathrm{d}}}^* + (i_{\mathrm{d0}} - {i_{\mathrm{d}}}^*)\frac{\mathrm{e}^{-\xi\omega_{\mathrm{h}}t}\sin(\omega_{\mathrm{d}}t + \beta)}{\sqrt{1-\xi^2}} \\ i_{\mathrm{q}} = {i_{\mathrm{q}}}^* - \frac{{i_{\mathrm{q}}}^*\mathrm{e}^{-\xi\omega_{\mathrm{h}}t}\sin(\omega_{\mathrm{d}}t + \beta)}{\sqrt{1-\xi^2}} \end{cases} \tag{8}$$

where

$$\begin{cases} \xi = k_{ip}/(2\sqrt{Lk_{ii}}) \\ \omega_{\mathrm{n}} = \sqrt{k_{ii}/L} \\ \omega_{\mathrm{d}} = \omega_{\mathrm{n}}\sqrt{1-\xi^2} \\ \beta = (\arctan\sqrt{1-\xi^2})/\xi \end{cases}$$

where

- ξ is the damping ratio of the second-order system;
- ω_{n} is the natural angular frequency of the second-order system;
- ω_{d} is the damped oscillation frequency;
- β is the damping angle, i_{d0} is the active current component before the fault.

After the transient components of the SCC have fully decayed, it can be observed from (6) that the SCC ultimately stabilizes to the reference current value. Combining the active power output before the fault and the inverter limiting, the calculation model of the fault steady-state SCC can be obtained as

$$\begin{cases} i_{\mathrm{d}} = {i_{\mathrm{d}}}^* = \min(i_{\mathrm{d0}}, {I_{\mathrm{dmax}}}^*) \\ i_{\mathrm{q}} = {i_{\mathrm{q}}}^* = 1.5(0.9 - U_{\mathrm{t}})I_{\mathrm{N}} \end{cases} \tag{9}$$

2.4. Influence Mechanism of SCC in AC System Connected to N-SMSs

As indicated by (5), under the LVRT control strategy, the N-SMSs can be regarded as a voltage-controlled current source. The higher the PCC voltage, the smaller the SCC produced by the N-SMSs. The PCC voltage is primarily influenced by the distance from the fault point to the PCC and the fault impedance. Therefore, for the same type of fault, the farther the fault is from the PCC and the greater the fault impedance, the higher the PCC voltage will be, and the smaller the SCC contribution from the N-SMSs will be.

3. Practical SCC Calculation Model for Renewable Power Plants

Renewable power plants contain a large number of N-SMSs, which are connected to the collection lines through step-up transformers at the machine terminals. Multiple collection lines converge into the interconnection lines, and then the power is integrated into the grid through a step-up substation. When a fault occurs in the power grid, causing a voltage sag, this voltage drop is transmitted through the lines to the terminals of the N-SMSs. Due to the presence of line and transformer impedance, as well as the spatial distribution of N-SMSs, the steady-state terminal voltage of each generator differs. Consequently, the steady-state SCCs injected after the fault also vary.

To obtain a more accurate estimation of steady-state SCC, it is necessary to determine the precise value of the steady-state terminal voltage. This paper first introduces a method for calculating the steady-state voltage at the point of grid connection during a fault. Based on this, a chained structure method is proposed for calculating the terminal fault steady-state voltage and SCC within renewable power plants. The detailed calculation method is introduced below.

The method presented in this paper is mainly applicable to the calculation of SCC during three-phase ground faults. In the case of LVRT, if an asymmetric fault occurs, relevant standards require the power plant to inject positive-sequence dynamic reactive current to support the recovery of positive-sequence voltage, while absorbing negative-sequence reactive current from the grid to suppress the rise of negative-sequence voltage. Therefore, the method in this paper does not apply to asymmetric faults. The following calculations are carried out under the positive-sequence network.

3.1. Determination of SCC Calculation Method

When a fault occurs outside the renewable power plant, the PCC voltage drops. The extent of this voltage drop determines whether the renewable power plant enters the LVRT mode. First, using the single-machine multiplication method, the renewable power plant is regarded as a large-capacity non-synchronous machine source. Initially assume that the renewable power plant enters the LVRT state during the fault. By considering the impact of reactive power on raising the PCC voltage and calculating U_{st} following the steps in Section 2.2, if $U_{\mathrm{st}} < 0.9$, the assumption is correct, and the calculation proceeds according to the method in Section 2.3. If $U_{\mathrm{st}} > 0.9$, the assumption is incorrect, meaning the renewable power plant has not entered the LVRT state, and the appropriate calculation method is selected according to the control strategy.

Based on the previous classification of N-SMSs, wind power and photovoltaic systems typically adopt PQ control or PV control.

If PQ control is used, because the P and Q command values remain unchanged during the fault, the PCC voltage is set to 0.9. Based on the following power and current equations, the maximum SCC can be calculated as

$$\begin{cases} P = \frac{3}{2}\left(u_{gd}i_d + u_{gq}i_q\right) = \frac{3}{2}U_g i_d \\ Q = \frac{3}{2}\left(u_{gq}i_d - u_{gd}i_q\right) = -\frac{3}{2}U_g i_q \end{cases} \quad (10)$$

If PV control is used, the control method is the same as that of a synchronous generator, and the SCC calculation method is the same as that for synchronous generators.

The determination process for the SCC calculation method is shown in Figure 5.

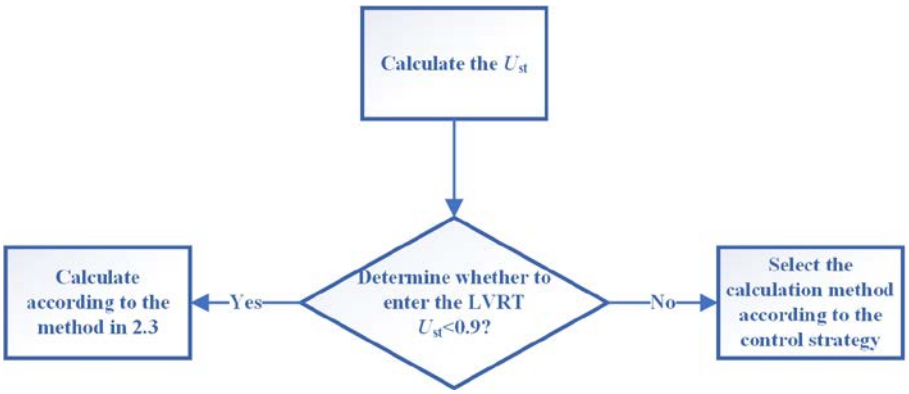

Figure 5. SCC calculation flowchart.

3.2. The Calculation Method for the Steady-State Voltage at the Point of Common Coupling (PCC)

The calculation method for the PCC voltage U_{st} shown in Figure 5 is as follows.

When a short-circuit fault occurs outside the renewable power plant, the renewable power plant can be regarded as a large voltage divider. The minimum depth of the PCC voltage drop is related to both the fault impedance and the system impedance [14,21]. A schematic diagram of an external fault at the renewable power plant is shown in Figure 6. The fault occurs at the location indicated by the red arrow.

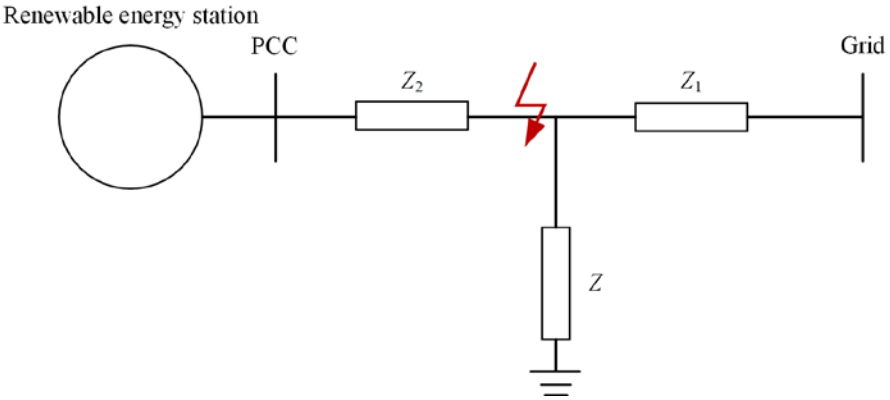

Figure 6. External fault of renewable power plant.

(1) Calculate the minimum depth of voltage drop using the short-circuit impedance:

$$U_{min} = \left|\frac{Z}{Z + Z_1}\right| E \quad (11)$$

where

- U_{min} is the amplitude of the PCC voltage at the moment of the fault;

- Z is the fault impedance;
- Z_1 is the impedance from the fault point to the system;
- E is the voltage amplitude of the infinite bus, which can be taken as a per unit value of 1.

In subsequent calculations, all variables are expressed in per unit values.

(2) The reactive current injected by the renewable power plant into the system will raise the PCC voltage [22]. Therefore, according to the superposition theorem, the steady-state voltage at the PCC can be expressed as follows:

$$U_{st} = U_{min} + \Delta U \tag{12}$$

where

- U_{st} is the steady-state voltage at the PCC during a fault in the renewable power plant;
- ΔU is the voltage rise caused by the reactive power injected into the system by the renewable power plant.

(3) During the fault steady-state period, neglecting the influence of active power on voltage and the resistance of the lines, the effect of reactive current on the voltage can be expressed as follows:

$$\Delta U = \frac{3}{2} I_{q\Sigma} \left(\frac{ZZ_1}{Z_1 + Z} + Z_2 \right) \tag{13}$$

where

- $I_{q\Sigma}$ is the reactive current provided by the renewable power plant during the fault;
- Z_2 is the impedance from the renewable power plant to the fault point.

(4) During the fault steady-state period, the reactive current is related to the terminal voltage of the generators. To simplify the calculations, ignore the differences between the various N-SMSs in the renewable power plant and use the single-machine multiplication method, treating the renewable energy source as a large-capacity N-SMSs. In this case, the reactive current provided by the renewable power plant can be expressed as follows:

$$I_{q\Sigma} = 1.5N(0.9 - U_{st})I_N \tag{14}$$

where

- N is the number of N-SMSs units within the renewable power plant.

(5) When the fault conditions and parameters of the renewable power plant are known, only I_q and U_{st} remain unknown in (9) to (12). By solving these equations simultaneously, the steady-state voltage at the PCC during the fault can be determined as follows:

$$\begin{cases} U_{st} = \frac{81NI_N Z_3 + 40U_{min}}{90NI_N Z_3 + 40} \\ Z_3 = \frac{ZZ_1}{Z_1 + Z} + Z_2 \end{cases} \tag{15}$$

3.3. SCC Calculation Method for Renewable Power Plants Under LVRT

In the steady state following a fault, N-SMSs can be treated as voltage-controlled current sources. With the PCC voltage known, determining the steady-state voltage at the generator terminals and the injected current becomes a power flow calculation problem. Power flow calculations typically use iterative methods, which can be complex. Given that renewable power plants often utilize chain or radial topologies [23], this paper proposes a simplified method for calculating steady-state SCCs based on these topological characteristics. The following outlines the calculation steps using the chain topology illustrated in Figure 7.

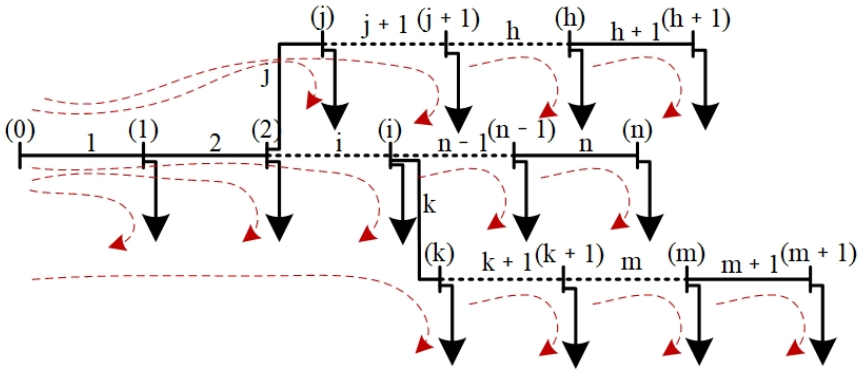

Figure 7. Renewable power plant internal loop.

(1) Number the internal lines and nodes of the renewable power plant.

Assign numbers to the internal lines and nodes of the renewable power plant. The first node in the system is the PCC, numbered as (0). The nodes representing N-SMSs are numbered sequentially. The line number corresponds to the number of the N-SMSs at the endpoint of that line.

(2) Construct the loop-branch incidence matrix $\boldsymbol{C}$.

Based on the topology, derive the loop-branch incidence matrix $\boldsymbol{C}$, where the rows represent loops and the columns represent branches. If a loop passes through a particular branch, the corresponding element in the matrix is set to 1; otherwise, it is set to 0. Using the line information, construct the loop-branch reactance matrix $\boldsymbol{X}$ as follows:

$$\boldsymbol{X}=\boldsymbol{C}\boldsymbol{X}_{\mathrm{l}} \tag{16}$$

where

- $\boldsymbol{X}_{\mathrm{l}}$ is the column vector of branch reactance.

(3) Calculate the terminal voltage of the N-SMSs.

The voltage equations between adjacent nodes are given by

$$U_i - U_j = \frac{3}{2} I_{\mathrm{qs}} X_i = \frac{3}{2} \sum I_x X_i \tag{17}$$

where

- U_{i} and U_{j} are the fault steady-state voltages of two adjacent non-synchronous power nodes.
- X_i is the line reactance of branch i,
- I_{qs} is the reactive current injected by node i + 1, which is the sum of the reactive current supplied by node i + 1 and the downstream asynchronous machine, and the reactive current generated by each asynchronous machine is determined by the low voltage crossing strategy, namely,

$$I_{\mathrm{qs}} = 1.5 \times (0.9 - U_x) I_{\mathrm{N}} \tag{18}$$

The linear Equations (13) and (14) for the machine terminal voltage can be listed as follows:

$$\begin{bmatrix} U_1 - U_0 \\ \vdots \\ U_i - U_j \\ \vdots \\ U_n - U_m \end{bmatrix} = \frac{9}{4} I_N \boldsymbol{C}^{\boldsymbol{T}} \begin{bmatrix} X_1(0.9 - U_1) \\ \vdots \\ X_i(0.9 - U_i) \\ \vdots \\ X_n(0.9 - U_n) \end{bmatrix} \tag{19}$$

(4) Calculate the SCC of the renewable power plant.

According to the terminal voltage and LVRT strategy, the SCC of each non-synchronous machine is calculated, and the SCC of the plant is obtained by summation.

$$\begin{cases} i_{d,i} = i_{d,i}^{*} = \min(i_{d0}, I_{dmax}^{*}) \\ i_{q,i} = i_{q,i}^{*} = 1.5(0.9 - U_i)I_N \end{cases} \tag{20}$$

$$I = \sum_{i=1}^{n} I_i \tag{21}$$

4. Results

In order to verify the feasibility of the method proposed in this paper, combined with the actual engineering, a detailed model of a renewable power plant, as shown in Figure 8, was built in PSCAD. The plant mainly includes a wind turbine, back-to-back converters, box converters and main converters. The wind turbine is connected to the box transformer (0.69 kV/35 kV) through back-to-back converters, then to the 35 kV bus through the collection line, and then to the 220 kV system through the main transformer (35 kV/220 kV). Due to the similarity of the collecting lines, the calculation example includes one collecting line with ten wind turbines, each rated at 2 MW capacity (permanent magnet direct drive). The spacing of the units is selected as 1 km, and the basic wind speed is set as 10 m/s. The main parameters of the wind farm are shown in Table 1. The grid-connected inverter adopts the control strategy shown in Figure 2. The fault occurs at the location indicated by the red arrow.

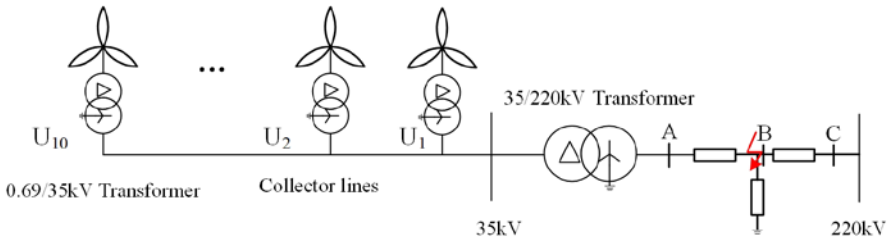

Figure 8. Sketch diagram of the detailed wind farm model.

Table 1. Main component parameters of permanent magnet wind field.

Type	Parameter	Value
35kV line	Impedance	0.13 + 0.23j Ω/km
Box-type transformer	Transformation ratio	0.69/35 kV
	Capacity	2.24 MW
	Impedance	6.39%
Main transformer	Transformation ratio	35/220 kV
	Capacity	100 MW
	Impedance	13.54%

The sum of the equivalent impedances of the AB and BC sections of the line is Z_{ac} = (2.43 + 6.91j) Ω. The impedance of the AB section is Z_{ab}, and let $\gamma = Z_{ab}/Z_{ac}$. By changing γ, the fault location can be adjusted. The greater the value of γ, the closer the fault is to the PCC. Set γ to 0.25, 0.5, and 0.75, and set the short-circuit impedance Z to 1 Ω, 2 Ω, and 3 Ω, respectively. A three-phase short-circuit fault is applied at t = 1 s, with the fault point located at point B marked by the red arrow in Figure 8. The fault lasts for 0.5 s.

The method proposed in Sections 3.1 and 3.2 was used to calculate the fault steady-state voltage at the end of each wind turbine in the wind farm, and the simulation results were compared, as shown in Figure 9 and Table 2. In Figure 9, the terminal voltage of the ten wind turbines at different fault locations and transition impedances is shown. The dashed lines represent the simulation results, and the solid lines represent the calculated values.

Table 2 shows the maximum relative error between the simulated and calculated voltage values of the wind turbines under different fault conditions. The calculation method for the relative error is as follows:

$$relative\ error\ = \frac{calculated\ value - simulated\ value}{simulated\ value} \times \mathbf{100}\%. \quad (22)$$

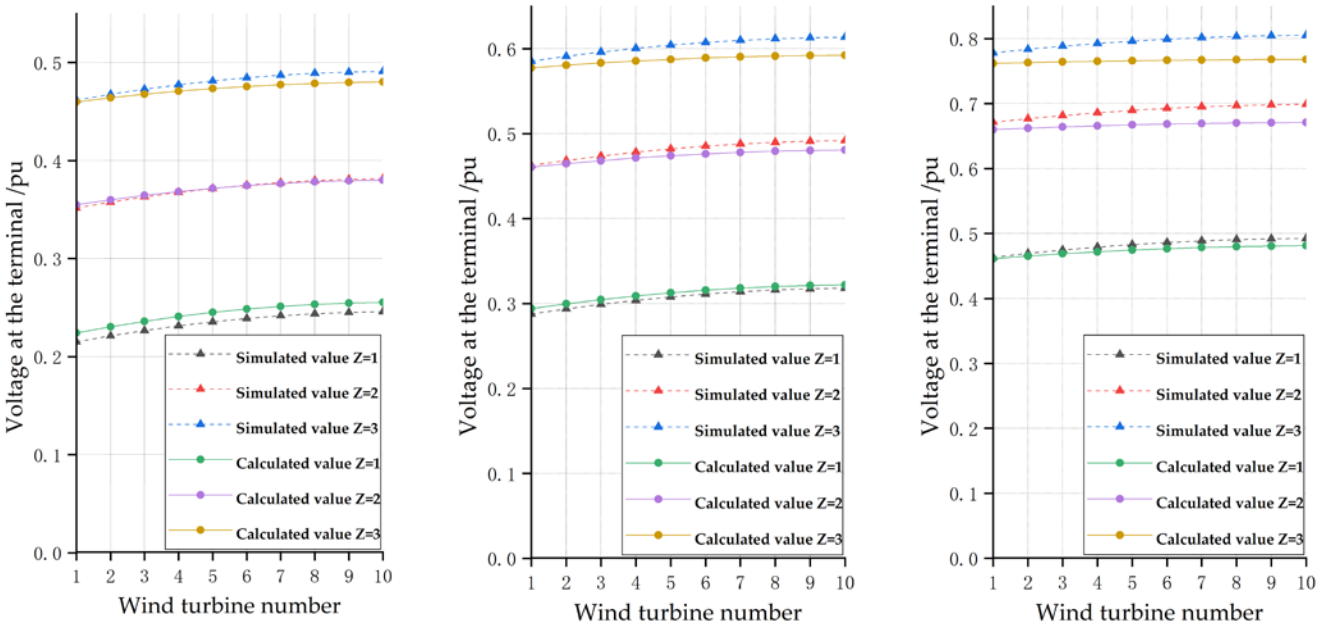

Figure 9. Fault steady-state voltage of each wind turbine in the different fault situations. (**a**) γ = 0.25; (**b**) γ = 0.50; (**c**) γ = 0.75.

Table 2. Maximum voltage error of wind.

γ	Short Circuit Impedance/Ω	Maximum Wind Turbine Voltage Relative Error/%
0.25	1	4.23
	2	0.95
	3	−2.20
0.50	1	2.24
	2	−2.26
	3	−3.44
0.75	1	−2.29
	2	−4.00
	3	−4.60

Table 3 presents the simulated SCC of the wind farm and PCC voltage under different fault conditions, the calculation values using the single-machine multiplication method, and the calculation values obtained using the method proposed in this paper. The calculation errors relative to the simulated values were also computed according to Equation (20).

Table 3. The short-circuit current of the wind farm.

γ	Short Circuit Impedance/Ω	PCC Voltage Simulated Value/p.u.	Simulated Value/kA	Single-Machine Multiplication Calculation Value/kA	Single-Machine Multiplication Relative Error/%	The Proposed Method Calculation Value/kA	The Proposed Method Relative Error/%
0.25	1	0.2086	0.4059	0.4223	4.04	0.4055	−0.11
	2	0.3451	0.3511	0.3583	2.03	0.3482	−0.84
	3	0.4552	0.2978	0.3098	4.01	0.3022	1.46
0.50	1	0.2808	0.3797	0.3878	2.12	0.3762	−0.92
	2	0.4561	0.2976	0.3095	4.02	0.3019	1.47
	3	0.5790	0.2478	0.2605	5.11	0.2556	3.16
0.75	1	0.4570	0.2975	0.3092	3.95	0.3017	1.40
	2	0.6651	0.2264	0.2309	1.97	0.2279	0.63
	3	0.7723	0.2028	0.2030	0.10	0.2019	−0.46

As shown in Figure 9, under a certain fault condition, the terminal voltages of the individual wind turbines are not identical, and the voltage increases as the distance from the grid connection point increases, which is due to the presence of line impedance. The figure also reveals the drawback of the single-machine multiplication method, which overlooks the internal differences within the wind farm, resulting in significant calculation errors. From Table 2, it can be seen that the maximum error between the method proposed in this paper and the simulated voltage does not exceed 5%, demonstrating the accuracy of the proposed method.

From Table 3, it can be seen that for the same fault location, as the fault impedance increases, the PCC voltage increases, and the SCC injected by the wind farm decreases. For the same fault impedance, the closer the fault point is to the PCC, the higher the PCC voltage and the smaller the SCC injected by the wind farm. Comparing the three conditions: $\gamma = 0.25$, $Z = 3$; $\gamma = 0.5$, $Z = 2$; and $\gamma = 0.75$, $Z = 1$, it is found that the PCC voltage is nearly the same in all three cases, and the SCC is also similar. This indicates that the SCC injected by the wind farm mainly depends on the PCC voltage.

From Table 3, it can be seen that the SCC accuracy obtained by the method proposed in this paper shows a significant improvement compared to the single-machine multiplication method, which verifies the feasibility of the method discussed in Section 2. When the internal differences within the wind farm are small, such as when there are only a few wind turbines connected to a single collection line, the terminal voltage variations between individual turbines are negligible, and the single-machine multiplication method can be used. However, as demonstrated in the example, when there are 10 turbines on a single line, the method proposed in this paper reduces the error by nearly half.

Compared to other iterative algorithms, the algorithm proposed in this paper has a time complexity that is linearly related to the number of wind turbines, without the issue of convergence. This significantly reduces the computational resources required.

5. Conclusions

Improved accuracy in fault detection and SCC estimation enhances the design, protection, and operation of renewable power plants. It allows for more reliable protection systems, reduced costs, and more efficient integration with the grid. These benefits not only improve the safety and economic performance of the wind farm but also contribute to a more resilient and stable power grid, which is critical as renewable energy becomes an increasingly larger part of global electricity generation. In the design of wind farm electrical protection systems, the accurate calculation of short-circuit currents is essential for the proper selection and sizing of protective devices. For instance, in a wind farm substation, circuit breakers are required to protect the electrical network connected to multiple wind turbines. If the short-circuit current is underestimated, engineers may inadvertently

choose circuit breakers with insufficient interrupting capacity. This miscalculation could result in delayed fault clearance, allowing fault conditions to persist longer, potentially causing significant damage to sensitive equipment, such as turbines or transformers, or even leading to cascading failures within the grid. Conversely, by employing accurate short-circuit current calculations, engineers can ensure that circuit breakers with appropriately rated interrupting capacities are selected. This enables timely fault detection and isolation, thereby enhancing system reliability and minimizing the risk of extensive equipment damage and grid instability. Such precision in short-circuit current estimation thus directly contributes to both the operational safety and cost-efficiency of the wind farm. An inaccurate short-circuit current estimate may lead to over-protection, resulting in frequent and unnecessary disconnections of renewable energy sources during transient conditions. By using more accurate calculations, engineers can reduce such occurrences, leading to less frequent power interruptions and better overall plant efficiency, which in turn improves economic returns by ensuring that the plant operates closer to its full potential.

According to the control strategy of the N-SMSs, the analytical expression of short-circuit current under LVRT has been derived in this paper. Then, according to the classification of the N-SMSs, a calculation method of fault steady-state voltage and short-circuit current of the N-SMSs in a renewable power plant without iterative calculation was proposed. The simulation results were verified using a single-machine infinite bus system and a real wind farm. The method is suitable for N-SMSs with different grid-connected strategies. The calculation principle is simple and no iteration is required, and the accuracy is greatly improved compared to single-machine multiplication, which provides a reference for the control and protection of renewable energy systems.

When using this model, attention must be given to the low penetration control strategy. The model derived in this paper is based on a case where $K_1 = 1.5$. In fact, the method remains applicable for other values of K_1; it only requires following the derivation steps accordingly. In this paper, when calculating the fault steady-state voltage of the junction point, the single machine was used to multiply, and only the reactive current was considered when the fault steady-state voltage and short-circuit current of the computer were considered, both of which affect the calculation accuracy. The method in this paper is only applicable to three-phase short-circuit faults. For other fault types, the requirements for positive-sequence and negative-sequence reactive current are different, so this method does not apply to asymmetric faults. For asymmetrical faults, sequence network analysis can be introduced to divide the power grid into positive, negative, and zero sequences. A positive-sequence short-circuit current has been analyzed in this paper. Negative-sequence short-circuit currents can be analyzed using a method similar to that used for the positive sequence. The zero-sequence short-circuit current is related to the transformer connection mode and whether the neutral point is grounded. Because the method proposed in this paper is based on a reactive-power-prioritized low penetration strategy, it is not applicable under other control strategies. Due to the insensitivity of node voltage to active power, the computational model presented in this paper can still be considered. However, attention should be paid to the analysis of errors when applying it.

The SCC under asymmetric faults and other LVRT control strategies can be further studied. How to reduce errors is a problem that needs further consideration.

Author Contributions: Writing—original draft, P.L.; Writing—review & editing, Y.H. and G.W.; Funding acquisition, J.L. (Jianhua Li) and J.L. (Jianyu Lu). All authors have read and agreed to the published version of the manuscript.

Funding: This research was funded by China East Branch of State Grid Corporation of China under the grant Research on the calculation model and method of short circuit current of renewable energy sources in new type power system, grant number 52992424001P.

Institutional Review Board Statement: Not applicable.

Informed Consent Statement: Not applicable.

Data Availability Statement: The original contributions presented in the study are included in the article, further inquiries can be directed to the corresponding author.

Conflicts of Interest: Authors Jianhua Li and Jianyu Lu were employed by the company China East Branch of State Grid Corporation of China. The remaining authors declare that the re-search was conducted in the absence of any commercial or financial relationships that could be construed as a potential conflict of interest.

References

1. Xie, X.; He, J.; Mao, H.; Li, H. New Issues and Classification of Power System Stability With High Shares of Renewables and Power Electronics. *Proc. CSEE* **2021**, *41*, 461–475. [CrossRef]
2. Jia, K.; Hou, L.; Liu, Q.; Fang, Y.; Zheng, L.; Bi, T. Analytical Calculation of Transient Current From an Inverter-Interfaced Renewable Energy. *IEEE Trans. Power Syst.* **2022**, *37*, 1554–1563. [CrossRef]
3. Yang, Z.; Jia, K.; Fang, Y.; Zhu, Z.; Yang, B.; Bi, T. High-Frequency Fault Component-Based Distance Protection for Large Renewable Power Plants. *IEEE Trans. Power Electron.* **2020**, *35*, 10352–10362. [CrossRef]
4. Li, R.; Gao, Q.; Liu, W. Characteristics of Direct-Driven Permanent Magnet Synchronous Wind Power Generator Under Symmetrical Three-Phase Short-Circuit Fault. *Power Syst. Technol.* **2011**, *35*, 153–158. [CrossRef]
5. Xu, K.; Zhang, Z.; Liu, H.; Liu, W.; Ao, J. Study on Fault Characteristics and Its Related Impact Factors of Photovoltaic Generator. *Trans. China Electrotech. Soc.* **2020**, *35*, 359–371. [CrossRef]
6. Kong, X.; Zhang, Z.; Yin, X.; Wang, F.; He, M. Study on Fault Current Characteristics and Fault Analysis Method of Power Grid With Inverter Interfaced Distributed Generation. *Proc. CSEE* **2013**, *33*, 65–74+13. [CrossRef]
7. Jia, K.; Zheng, L.; Bi, T.; Yang, Z.; Li, Y.; Han, J. Pilot Protection Based on Cosine Similarity for Transmission Line Connected to Wind Farms. *Proc. CSEE* **2019**, *39*, 6263–6275. [CrossRef]
8. Li, B.; Zhang, H.; Duan, Z.; Lin, M. Analysis of the Effect of Control Strategy on the Fault Transient Characteristics of Inverter-based Distributed Generators. *Proc. CSU-EPSA* **2014**, *26*, 1–7+27. [CrossRef]
9. Song, J.; Cheah-Mane, M.; Prieto-Araujo, E.; Gomis-Bellmunt, O. Short-Circuit Analysis of AC Distribution Systems Dominated by Voltage Source Converters Considering Converter Limitations. *IEEE Trans. Smart Grid* **2022**, *13*, 3867–3878. [CrossRef]
10. Yin, J.; Bi, T.; Xue, A.; Yang, Q. Study on Short-circuit Current and Fault Analysis Method of Hybrid Wind Farm with Low Voltage Ride-through Control Strategy. *Trans. China Electrotech. Soc.* **2015**, *30*, 99–110. [CrossRef]
11. Jia, K.; Hou, L.; Bi, T.; Li, Y.; Qing, H.; Ding, X. Practical Engineering Calculation of Short-circuit Current for Renewable Energy Based on Local Iteration of Fault Area. *Autom. Electr. Power Syst.* **2021**, *45*, 151–158. [CrossRef]
12. Zou, J.; Peng, C.; Xu, H.; Yan, Y. A Fuzzy Clustering Algorithm-Based Dynamic Equivalent Modeling Method for Wind Farm With DFIG. *IEEE Trans. Energy Convers.* **2015**, *30*, 1329–1337. [CrossRef]
13. Meng, H.; Ye, X.; Yang, M.; Song, X.; Su, Z.; Liu, W.; Luo, L.; Zhao, H. Equivalent modeling and simulation for PV system on dynamic clustering equivalent strategy. In Proceedings of the IECON 2017—43rd Annual Conference of the IEEE Industrial Electronics Society, Beijing, China, 29 October–1 November 2017; pp. 5779–5784. [CrossRef]
14. Li, D.; Shen, C.; Wu, L.; Chen, X.; Yang, Y. Study on Fault Response Characteristics Classification and Discriminant Method of PMSG Considering Initial Wind Speed and Drop Degree of Terminal Fault Steady-state Voltage. *Proc. CSEE* **2024**, *44*, 1247–1260. [CrossRef]
15. Tang, Y.; Song, G.; Hao, Z.; Jiang, J.; Chang, N.; Lang, X. Practical Calculation Method for Fault Steady-state Current in Inverter-interfaced Generator Stations. *Autom. Electr. Power Syst.* **2024**, *48*, 182–191. [CrossRef]
16. Luo, Y.; Tang, H.; Li, J.; Hou, S.; Xue, A. A short-circuit current calculation method for direct-driven wind farms based on voltage iteration. *Zhejiang Electr. Power* **2024**, *43*, 75–84. [CrossRef]
17. Wu, C.; Xiao, S. Quasi-newton iterative calculation method for short circuit current of high proportion distributed generation connected to power grid. *Power Syst. Technol.* **2022**, *46*, 4581–4590. [CrossRef]
18. Xu, Z. Reasonable Definition and Calculation Method of Power Grid Strength Under the Background of New Type Power Systems. *High Volt. Eng.* **2022**, *48*, 3805–3819. [CrossRef]
19. *GB/T 19963.1-2021*; Technical Specification for Connecting Wind Farm to Power System. Part 1: On Shore Wind Power. Standards Press of China: Beijing, China, 2021.
20. Li, W. *Research on Wind Farm Fault Characteristics and Its Short Circuit Current Calculation Model*; North China Electric Power University: Beijing, China, 2018.
21. Sun, H.; Li, J.; Li, W.; Guo, J.; An, N.; Zhang, Y. Research on Model Structures and Modeling Methods of Renewable Energy Station for Large-scale Power System Simulation (II): Electromechanical Transient Model. *Proc. CSEE* **2023**, *43*, 2190–2202. [CrossRef]
22. He, J.; Zhuang, W.; Xu, T.; Huo, C.; Jiang, W. Study on Cascading Tripping Risk of Wind Turbines Caused by Transient Overvoltage and Its Countermeasures. *Power Syst. Technol.* **2016**, *40*, 1839–1844. [CrossRef]
23. Yang, Y. *Study on Topology Structure of Large Wind Power Base*; North China Electric Power University: Beijing, China, 2017.